Int. J. Solids Structures Vol. 17, pp. 11–27
Pergamon Press Ltd., 1981. Printed in Great Britain

POST-CRITICAL ANALYSIS OF TORSIONALLY BUCKLED STIFFENER PLATES

C. P. ELLINAS and J. G. A. CROLL
Civil and Municipal Engineering Department, University College London, Gower Street London, WCIE 6BT, England

(*Received* 9 *April* 1980)

Abstract—The determination of the moment-curvature characteristics for stiffened plates buckling away from slender stiffener outstands is seen as an important step towards developing simple engineering approaches to the design problem.

The main aspects of a recent programme of research carried out to provide this information on moment-curvature relationships are presented here. A non-linear large deflection analysis of an analytical model has been developed, in which the non-linear equilibrium and boundary conditions are reduced to a linear form by employing a perturbation scheme, and then discretized using pertinent difference expressions. Finally the sequence followed for the solution of the resulting linear simultaneous algebraic equations is outlined.

The validity of this analysis has been demonstrated by comparing the theoretical results with typical results taken from an extensive series of experiments. Some of the important mechanics of behaviour and their implications are also discussed.

1. INTRODUCTION

There has over the past decade been a rapid increase in the use of thin stiffness steel panels in Civil Engineering structures. In box girder bridges and in even larger scale in marine structures the economies that can be achieved in the use and careful design of such components are considerable. But at the same time, as this process of optimization is continued, the forms of behaviour of these systems become increasingly complicated.

Van der Neut[1] was the first to examine analytically the problem of mode interaction arising when the local and overall critical modes of a class of box columns occur at approximately the same load levels. His demonstration of the unstable and consequently imperfection sensitive buckling that can occur in these systems drew attention to an effect that had been intuitively understood for wide classes of structures for a much longer time. The result has been an increasing research effort towards understanding more fully the nature of the mechanics displayed by simultaneous and near simultaneous buckling of structures composed of plates, especially that of the stiffened plate [2–4].

One of the major problems for the designer of systems of this type is that a complete understanding of their behaviour can only be achieved through the solution of highly non-linear differential equations. It has not always been terribly clear how the approximate solutions of these governing equations would relate to the forms of behaviour displayed by practical structures. This, coupled with the fact that failure when it occurs is violent and with little warning that is about to occur, makes it understandable why in design recommendations there has been a tendency to avoid those parametric ranges that produce such conditions[5]. But in consequence the parametric ranges that offer the greatest potential for improving efficiency are also being avoided.

One approach to the design of these systems that avoids the necessity of performing these complex forms of interactive postbuckling analysis, is that based on the use of the reduced modulus load [6, 7]. This has now been fully described for the case of the box column and stiffened plate buckling towards the stiffener outstands [6–8]. However, for the case of a plate buckling away from slender stiffener outstands that are prone to local torsional buckling, see Fig. 1, the necessary information on the moment-curvature characteristics is as yet not fully available. The research[9] upon which the following is based has as its aim the provision of this information.

In what follows the non-linear large deflection equations governing the behaviour of a simplified model of a typical section of a stiffened panel are reviewed. Employing a continuum perturbation scheme the non-linear differential equations are reduced to the form of a sequence of linear equations that are subsequently solved using approximate finite difference methods.

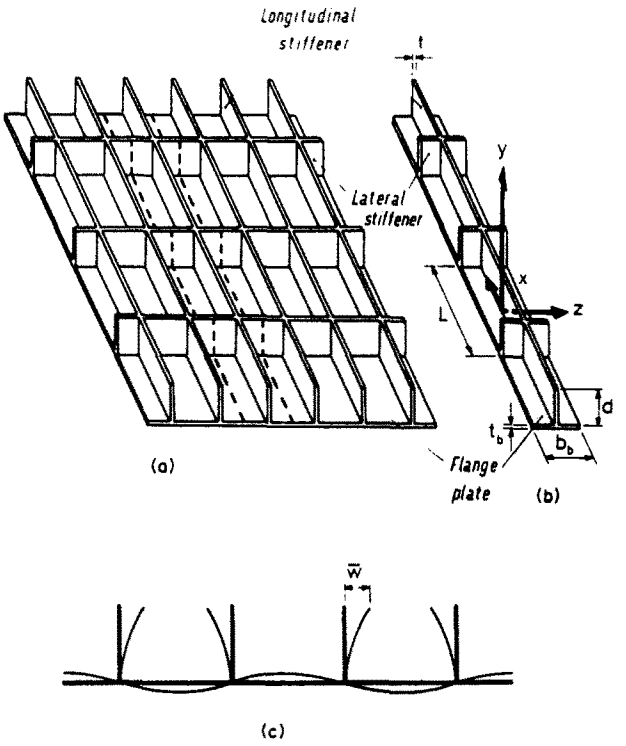

Fig. 1. Asymmetrically stiffened plate.

Verification of the numerical solution is established by comparisons with a selection of results from a wide ranging experimental programme. Extensive parametric studies[9] based on this analysis have provided a rational basis for the optimum design of plates stiffened with slender outstands.

2. THE PHYSICAL MODEL

The model used is a rectangular plate that has beam supports on both the top and bottom boundaries, with kinematic conditions assumed on the end boundaries. The system is subjected to in-plane stresses on its ends that produce a controlled ratio between the overall moment, M and the axial load, P. To ensure that the bottom edge beam adequately models the action of the flange of stiffened plates, the out-of-plane displacement at the bottom support is taken to be zero. The object is to investigate for this model the relationship between the overall moment, M and the corresponding overall curvature change, κ, under different axial loads, P.

This model can be considered as the basic unit of a stiffened plate like that shown in Fig. 1. When a wide stiffened plate of this type is subjected to a uniform axial loading, a typical longitudinal stiffener, shown in Fig. 1(b), will buckle locally in the manner illustrated in Fig. 1(c). Once this occurs the overall flexural stiffness, EI, of a typical stiffener will have been reduced to ηEI. It is the factor η that is referred to as the "reduced modulus factor". Its importance in controlling the incremental behaviour of imperfect systems of this type is now well established. To determine η for the present system it is enough to consider the section of stiffener plate between two consecutive transverse stiffeners. In this context, therefore, the top edge beam, shown in Fig. 2, would represent the possible edge stiffening on the stiffener

longitudinal and transverse stiffeners.

3. THEORETICAL MODEL

The analysis that follows is based on the von Karman large deflections theory of thin plates. With the convention for positive stress and moment resultants acting on a typical plate element,

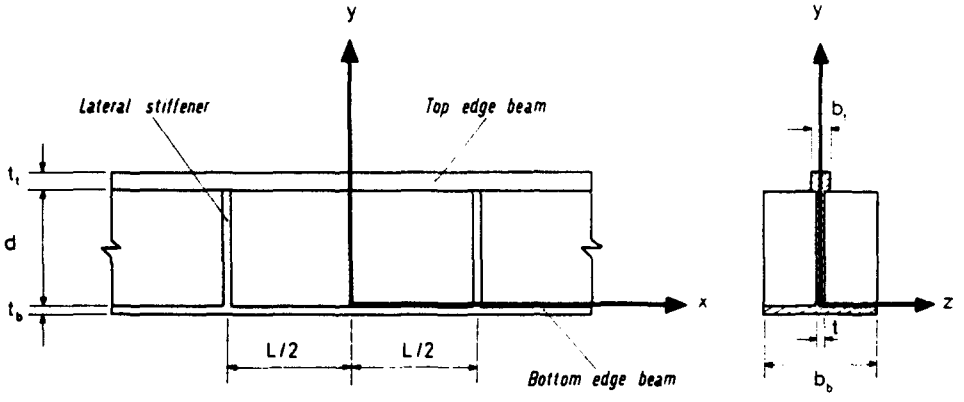

Fig. 2. Simplified analytical model.

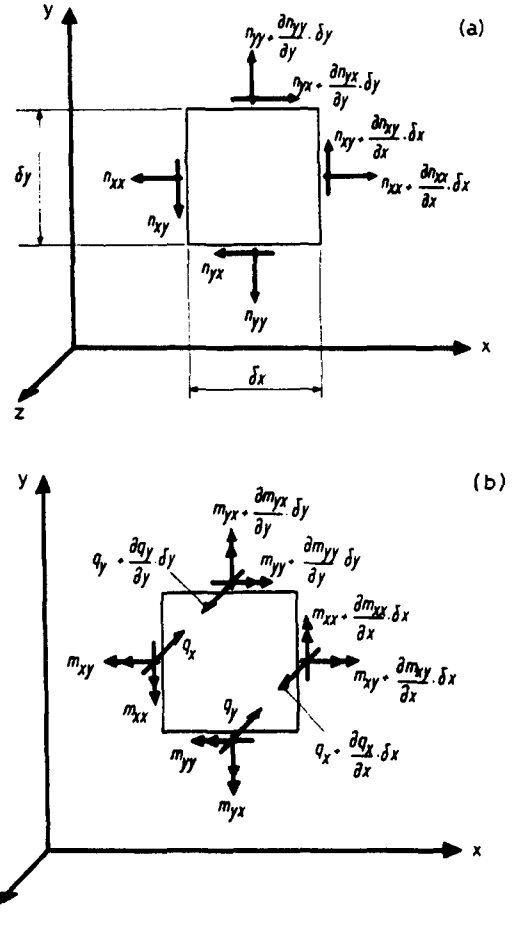

Fig. 3. Notation and positive convention for plate element actions.

shown in Fig. 3, the plate mid-surface stress and moment resultants may be written

$$n_{xx} = k\left[\frac{\partial U}{\partial x} + \frac{1}{2}\left(\frac{\partial W}{\partial x}\right)^2 + \nu\frac{\partial V}{\partial y} + \frac{1}{2}\nu\left(\frac{\partial W}{\partial y}\right)^2\right] \tag{1a}$$

$$n_{yy} = k\left[\frac{\partial V}{\partial y} + \frac{1}{2}\left(\frac{\partial W}{\partial y}\right)^2 + \nu\frac{\partial U}{\partial x} + \frac{1}{2}\nu\left(\frac{\partial W}{\partial x}\right)^2\right] \tag{1b}$$

$$n_{xy} = \frac{1}{2}(1-\nu)k\left[\frac{\partial U}{\partial y} + \frac{\partial V}{\partial x} + \frac{\partial W}{\partial x}\frac{\partial W}{\partial y}\right] = n_{yx} \tag{1c}$$

$$m_{xx} = -D\left[\frac{\partial^2 W}{\partial x^2} + \nu\frac{\partial^2 W}{\partial y^2}\right] \tag{2a}$$

$$m_{yy} = D\left[\frac{\partial^2 W}{\partial y^2} + \nu\frac{\partial^2 W}{\partial x^2}\right] \tag{2b}$$

$$m_{xy} = D(1-\nu)\frac{\partial^2 W}{\partial x \partial y} = -m_{yx} \tag{2c}$$

$$q_y = -D\left[\frac{\partial^3 W}{\partial y^3} + \frac{\partial^3 W}{\partial x^2 \partial y}\right]. \tag{2d}$$

When substituted into the force and moment equilibrium equations for the plate element shown in Fig. 3, the six equilibrium equations may be reduced to the non-linear thin plate equilibrium equations

$$\frac{\partial^2 U}{\partial x^2} + \frac{1-\nu}{2}\frac{\partial^2 U}{\partial y^2} + \frac{1+\nu}{2}\frac{\partial^2 V}{\partial x \partial y} + \frac{\partial W}{\partial x}\frac{\partial^2 W}{\partial x^2} + \frac{1-\nu}{2}\frac{\partial W}{\partial x}\frac{\partial^2 W}{\partial y^2} + \frac{1+\nu}{2}\frac{\partial W}{\partial y}\frac{\partial^2 W}{\partial x \partial y} = 0 \tag{3a}$$

$$\frac{\partial^2 V}{\partial y^2} + \frac{1-\nu}{2}\frac{\partial^2 V}{\partial x^2} + \frac{1+\nu}{2}\frac{\partial^2 U}{\partial x \partial y} + \frac{\partial W}{\partial y}\frac{\partial^2 W}{\partial y^2} + \frac{1-\nu}{2}\frac{\partial W}{\partial y}\frac{\partial^2 W}{\partial x^2} + \frac{1+\nu}{2}\frac{\partial W}{\partial x}\frac{\partial^2 W}{\partial x \partial y} = 0 \tag{3b}$$

$$D\nabla^4 W - k\left[\frac{\partial U}{\partial x} + \frac{1}{2}\left(\frac{\partial W}{\partial x}\right)^2 + \nu\frac{\partial V}{\partial y} + \frac{1}{2}\nu\left(\frac{\partial W}{\partial y}\right)^2\right]\frac{\partial^2 W}{\partial x^2} - (1-\nu)k\left[\frac{\partial U}{\partial y} + \frac{\partial V}{\partial x} + \frac{\partial W}{\partial x}\frac{\partial W}{\partial y}\right]\frac{\partial^2 W}{\partial x \partial y}$$

$$- k\left[\frac{\partial V}{\partial y} + \frac{1}{2}\left(\frac{\partial W}{\partial y}\right)^2 + \nu\frac{\partial U}{\partial x} + \frac{1}{2}\nu\left(\frac{\partial W}{\partial x}\right)^2\right]\frac{\partial^2 W}{\partial y^2} = 0. \tag{3c}$$

Here (U, V, W) are the mid-surface displacements in the (x, y, z) coordinate directions, $\nabla^4 W$ is the biharmonic operator and

$$k = \frac{Et}{(1-\nu^2)} \tag{4a}$$

$$D = \frac{Et^3}{12(1-\nu^2)} \tag{4b}$$

are respectively the extensional and flexural rigidities of the plate, with modulus of elasticity, E and Poisson's ratio, ν.

Equilibrium considerations of the top edge beam, shown in Fig. 4, taking into account the effects of the plate stress and moment resultants acting on the beam-plate intersection, requires

$$\frac{\partial N_x}{\partial x} - n_{yx} = 0 \tag{5a}$$

$$\frac{\partial M_x}{\partial x} - m_{yy} + \frac{t_t}{2}\left(q_y + n_{yy}\frac{\partial W}{\partial y} + n_{yx}\frac{\partial W}{\partial x}\right) = 0 \tag{5b}$$

$$\frac{\partial^2 M_y}{\partial x^2} + N_x\frac{\partial^2 W_t}{\partial x^2} - \left(q_y + \frac{\partial m_{yx}}{\partial x} + n_{yy}\frac{\partial W}{\partial y}\right) = 0 \tag{5c}$$

$$\frac{\partial^2 Mz}{\partial x^2} + n_{yy} - \frac{t_t}{2}\frac{\partial n_{yx}}{\partial x} = 0 \tag{5d}$$

Subscript t refers to displacements computed at the top beam centroidal axis. With the edge beam axial force and moments related to these displacements given by

$$N_x = EA_t\left[\frac{\partial U_t}{\partial x} + \frac{1}{2}\left(\frac{\partial W_t}{\partial x}\right)^2\right] \tag{6a}$$

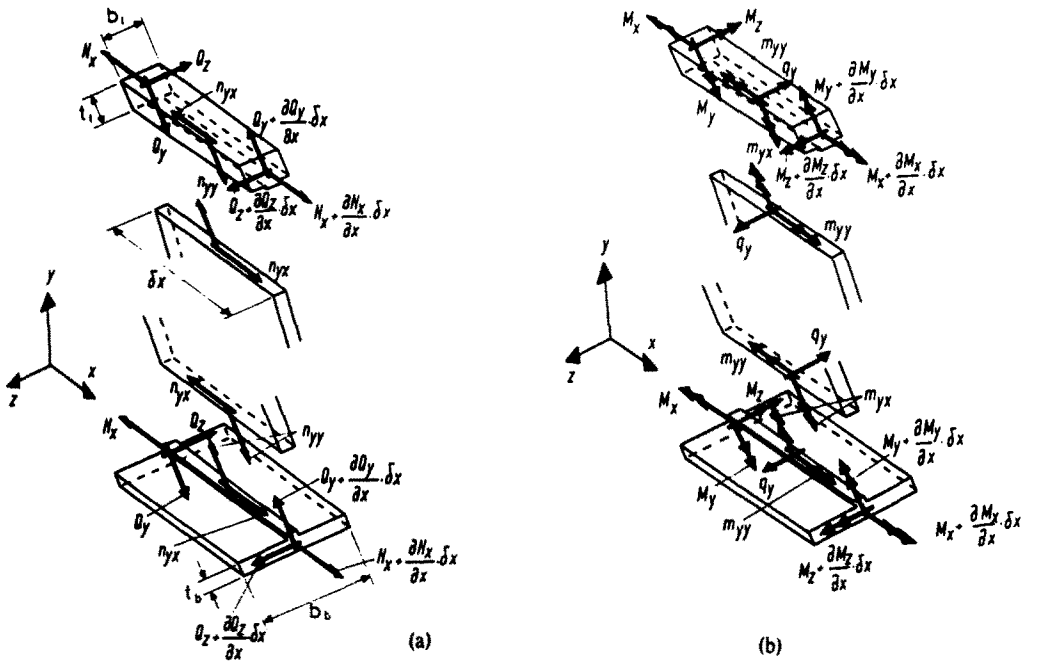

Fig. 4. Notation and positive convention for beam element actions.

$$M_x = GJ_t \frac{\partial^2 W_t}{\partial x \partial y} \tag{6b}$$

$$M_y = -EI_{yyt} \frac{\partial^2 W_t}{\partial x^2} \tag{6c}$$

$$M_z = EI_{zzt} \frac{\partial^2 V_t}{\partial x^2} \tag{6d}$$

and with the compatibility of the top beam-plate intersection and centroidal axis displacements requiring[9]

$$U_t = U - \frac{t_t}{2}\frac{\partial V}{\partial x} \tag{7}$$

$$V_t = V \tag{7b}$$

$$W_t = W + \frac{t_t}{2}\frac{\partial W}{\partial y} \tag{7c}$$

$$\frac{\partial W_t}{\partial y} = \frac{\partial W}{\partial y} \tag{7d}$$

the edge beam-plate interaction conditions (5) become

$$EA_t\left[\frac{\partial^2 U}{\partial x^2} - \frac{t_t}{2}\frac{\partial^3 V}{\partial x^3} + \left(\frac{\partial W}{\partial x} + \frac{t_t}{2}\frac{\partial^2 W}{\partial x \partial y}\right)\left(\frac{\partial^2 W}{\partial x^2} + \frac{t_t}{2}\frac{\partial^3 W}{\partial x^2 \partial y}\right)\right] - \frac{1}{2}(1-\nu)k\left[\frac{\partial U}{\partial y} + \frac{\partial V}{\partial x} + \frac{\partial W}{\partial x}\frac{\partial W}{\partial y}\right] = 0 \tag{8a}$$

$$GJ_t\frac{\partial^3 W}{\partial x^2 \partial y} - D\left[\frac{\partial^2 W}{\partial y^2} + \nu\frac{\partial^2 W}{\partial x^2}\right] - \frac{t_t}{2}\left\{D\left[\frac{\partial^3 W}{\partial y^3} + \frac{\partial^3 W}{\partial x^2 \partial y}\right] - k\left[\frac{\partial V}{\partial y} + \frac{1}{2}\left(\frac{\partial W}{\partial y}\right)^2 + \nu\frac{\partial U}{\partial x} + \frac{1}{2}\nu\left(\frac{\partial W}{\partial x}\right)^2\right]\frac{\partial W}{\partial y} - \frac{1}{2}(1-\nu)k\left[\frac{\partial U}{\partial y} + \frac{\partial V}{\partial x} + \frac{\partial W}{\partial x}\frac{\partial \dot{W}}{\partial y}\right]\frac{\partial W}{\partial x}\right\} = 0 \tag{8b}$$

$$-EI_{yyt}\frac{\partial^4 W}{\partial x^4}+D\left[\frac{\partial^3 W}{\partial y^3}+(2-\nu)\frac{\partial^3 W}{\partial x^2\partial y}\right]$$
$$+EA_t\left[\frac{\partial U}{\partial x}-\frac{t_t}{2}\frac{\partial^2 V}{\partial x^2}+\frac{1}{2}\left(\frac{\partial W}{\partial x}+\frac{t_t}{2}\frac{\partial^2 W}{\partial x\partial y}\right)^2\right]\left(\frac{\partial^2 W}{\partial x^2}+\frac{t_t}{2}\frac{\partial^3 W}{\partial x^2\partial y}\right)$$
$$-k\left[\frac{\partial V}{\partial y}+\frac{1}{2}\left(\frac{\partial W}{\partial y}\right)^2+\nu\frac{\partial U}{\partial x}+\frac{1}{2}\nu\left(\frac{\partial W}{\partial x}\right)^2\right]\frac{\partial W}{\partial y}=0 \tag{8c}$$

$$EI_{zzt}\frac{\partial^4 V}{\partial x^4}+k\left[\frac{\partial V}{\partial y}+\frac{1}{2}\left(\frac{\partial W}{\partial y}\right)^2+\nu\frac{\partial U}{\partial x}+\frac{1}{2}\nu\left(\frac{\partial W}{\partial x}\right)^2\right]$$
$$-\frac{t_t}{4}(1-\nu)k\left[\frac{\partial^2 U}{\partial x\partial y}+\frac{\partial^2 V}{\partial x^2}+\frac{\partial^2 W}{\partial x^2}\frac{\partial W}{\partial y}+\frac{\partial W}{\partial x}\frac{\partial^2 W}{\partial x\partial y}\right]=0. \tag{8d}$$

In these top boundary conditions the unsubscripted displacements are those at the edge beam-plate intersection; A_t is the cross-sectional area, GJ_t is the torsional stiffness and I_{yyt}, I_{zzt} the second moments of area of the top beam about the y and z axes respectively.

Following the procedure established for the top beam support, but making the assumption that the bottom beam has a bending stiffness about the y-axis which is very large in comparison with that of the plate, the plate edge conditions at the bottom longitudinal boundary may be written

$$EA_b\left[\frac{\partial^2 U}{\partial x^2}+\frac{t_b}{2}\frac{\partial^3 V}{\partial x^3}\right]+\frac{1}{2}(1-\nu)k\left[\frac{\partial U}{\partial y}+\frac{\partial V}{\partial x}+\frac{\partial W}{\partial x}\frac{\partial W}{\partial y}\right]=0 \tag{9a}$$

$$GJ_b\frac{\partial^3 W}{\partial x^2\partial y}+D\left[\frac{\partial^2 W}{\partial y^2}+\nu\frac{\partial^2 W}{\partial x^2}\right]-\frac{t_b}{2}\left\{D\left[\frac{\partial^3 W}{\partial y^3}+\frac{\partial^3 W}{\partial x^2\partial y}\right]\right.$$
$$-k\left[\frac{\partial V}{\partial y}+\frac{1}{2}\left(\frac{\partial W}{\partial y}\right)^2+\nu\frac{\partial U}{\partial x}+\frac{1}{2}\nu\left(\frac{\partial W}{\partial x}\right)^2\right]\frac{\partial W}{\partial y}$$
$$\left.-\frac{1}{2}(1-\nu)k\left[\frac{\partial U}{\partial y}+\frac{\partial V}{\partial x}+\frac{\partial W}{\partial x}\frac{\partial W}{\partial y}\right]\frac{\partial W}{\partial x}\right\}=0 \tag{9b}$$

$$W-\frac{t_b}{2}\frac{\partial W}{\partial y}=0 \tag{9c}$$

$$EI_{zzb}\frac{\partial^4 V}{\partial x^4}-k\left[\frac{\partial V}{\partial y}+\frac{1}{2}\left(\frac{\partial W}{\partial y}\right)^2+\nu\frac{\partial U}{\partial x}+\frac{1}{2}\nu\left(\frac{\partial W}{\partial x}\right)^2\right]$$
$$-\frac{t_b}{4}(1-\nu)k\left[\frac{\partial^2 U}{\partial x\partial y}+\frac{\partial^2 V}{\partial x^2}+\frac{\partial^2 W}{\partial x^2}\frac{\partial W}{\partial y}+\frac{\partial W}{\partial x}\frac{\partial^2 W}{\partial x\partial y}\right]=0. \tag{9d}$$

Again, displacements are those at the edge beam-plate intersection, while all geometric quantities for the bottom beam have the subscript b, and have the same meanings as for the top beam. It is perhaps worth noting that a free top longitudinal plate edge condition is obtained when the top beam dimensions are put equal to zero. With the bottom beam dimensions equal to zero, the bottom plate edge conditions would reduce to those of the classical simple support.

At the ends the boundary conditions are assumed to be

$$U-\alpha-\beta\frac{y}{d}=0 \tag{10a}$$

$$V=0 \tag{10b}$$

$$W=0 \tag{10c}$$

$$\frac{\partial^2 W}{\partial x^2}=0 \tag{10d}$$

where α and β are constants representing translation and rotation of the end supports respectively. They are defined by prescribing the axial force, P and the bending moment, M, due to the externally applied force system.

4. CONTINUUM PERTURBATION ANALYSIS

The above non-linear equilibrium and boundary differential equations are converted into an infinite set of linear differential equations by employing a continuum perturbation method[10]. For this, it is assumed that a single equilibrium path, P_1, emerges from the unloaded state (M, U, V, W) = (0, 0, 0, 0). Displacement components on this fundamental path, shown in Fig. 5(a), are distinguished by the superscript F and are assumed to vary linearly with M. Equilibrium equations (3) when evaluated on path P_1 become

$$\frac{\partial^2 U^F}{\partial x^2}+\frac{1-\nu}{2}\frac{\partial^2 U^F}{\partial y^2}+\frac{1+\nu}{2}\frac{\partial^2 V^F}{\partial x\partial y}=0 \tag{11a}$$

$$\frac{\partial^2 V^F}{\partial y^2}+\frac{1-\nu}{2}\frac{\partial^2 V^F}{\partial x^2}+\frac{1+\nu}{2}\frac{\partial^2 U^F}{\partial x\partial y}=0 \tag{11b}$$

$$W^F=0 \tag{11c}$$

which together with the appropriate linearisation of the boundary conditions (8)–(10) yield the fundamental path displacements (U^F, V^F, W^F).

A secondary path P_2 emanating from a critical state C, shown in Fig. 5(a), is then most conveniently studied by introducing the sliding transformations

$$U=U^F(M,x,y)+u(x,y) \tag{12a}$$

$$V=V^F(M,x,y)+v(x,y) \tag{12b}$$

$$W=w(x,y) \tag{12c}$$

where (U, V, W) are total displacements, (U^F, V^F, W^F) are the fundamental path displacements and (u, v, w) are the transformed displacements. This has the effect of mapping path P_1 onto the M-axis, as shown in Fig. 5(b). Substitution of the mapping eqns (12) into the equilibrium equations and using eqns (11), transforms eqns (3) into the form

$$\frac{\partial^2 u}{\partial x^2}+\frac{1-\nu}{2}\frac{\partial^2 u}{\partial y^2}+\frac{1+\nu}{2}\frac{\partial^2 v}{\partial x\partial y}+\frac{\partial w}{\partial x}\frac{\partial^2 w}{\partial x^2}+\frac{1-\nu}{2}\frac{\partial w}{\partial x}\frac{\partial^2 w}{\partial y^2}+\frac{1+\nu}{2}\frac{\partial w}{\partial y}\frac{\partial^2 w}{\partial x\partial y}=0 \tag{13a}$$

$$\frac{\partial^2 v}{\partial y^2}+\frac{1-\nu}{2}\frac{\partial^2 v}{\partial x^2}+\frac{1+\nu}{2}\frac{\partial^2 u}{\partial x\partial y}+\frac{\partial w}{\partial y}\frac{\partial^2 w}{\partial y^2}+\frac{1-\nu}{2}\frac{\partial w}{\partial y}\frac{\partial^2 w}{\partial x^2}+\frac{1+\nu}{2}\frac{\partial w}{\partial x}\frac{\partial^2 w}{\partial x\partial y}=0 \tag{13b}$$

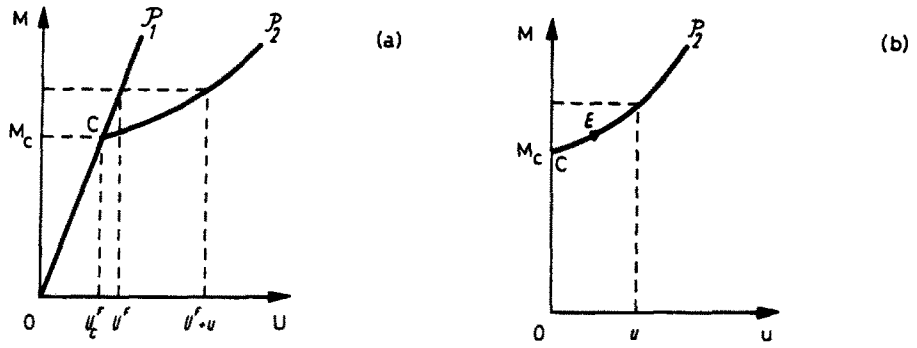

Fig. 5. (a) Original and (b) transformed equilibrium paths.

$$D\nabla^4 w - M\left[n^F_{xx,m}\frac{\partial^2 w}{\partial x^2} + 2n^F_{xy,m}\frac{\partial^2 w}{\partial x\partial y} + n^F_{yy,m}\frac{\partial^2 w}{\partial y^2}\right]$$
$$-k\left[\frac{\partial u}{\partial x} + \frac{1}{2}\left(\frac{\partial w}{\partial x}\right)^2 + \nu\frac{\partial v}{\partial y} + \frac{1}{2}\nu\left(\frac{\partial w}{\partial y}\right)^2\right]\frac{\partial^2 w}{\partial x^2}$$
$$-(1-\nu)k\left[\frac{\partial u}{\partial y} + \frac{\partial v}{\partial x} + \frac{\partial w}{\partial x}\frac{\partial w}{\partial y}\right]\frac{\partial^2 w}{\partial w\partial y}$$
$$-k\left[\frac{\partial v}{\partial y} + \frac{1}{2}\left(\frac{\partial w}{\partial y}\right)^2 + \nu\frac{\partial u}{\partial x} + \frac{1}{2}\nu\left(\frac{\partial w}{\partial x}\right)^2\right]\frac{\partial^2 w}{\partial y^2} = 0 \tag{13c}$$

where

$$n^F_{xx,m} = \frac{dn^F_{xx}}{dM}, \ldots\ldots$$

Progress along a prospective secondary path P_2, measured from the critical state C, is represented by the parameter ϵ. With eqns (13) satisfied for all ϵ along the path P_2, it follows that their derivatives with respect to ϵ, evaluated at the critical state, must also be satisfied. The first order derivative yields

$$\frac{\partial^2 u_{,1}}{\partial x^2} + \frac{1-\nu}{2}\frac{\partial^2 u_{,1}}{\partial y^2} + \frac{1+\nu}{2}\frac{\partial^2 v_{,1}}{\partial x\partial y} = 0 \tag{14a}$$

$$\frac{\partial^2 v_{,1}}{\partial y^2} + \frac{1-\nu}{2}\frac{\partial^2 v_{,1}}{\partial x^2} + \frac{1+\nu}{2}\frac{\partial^2 u_{,1}}{\partial x\partial y} = 0 \tag{14b}$$

$$D\nabla^4 w_{,1} - M_c\left[n^F_{xx,m}\frac{\partial^2 w_{,1}}{\partial x^2} + 2n^F_{xy,m}\frac{\partial^2 w_{,1}}{\partial x\partial y} + n^F_{yy,m}\frac{\partial^2 w_{,1}}{\partial y^2}\right] = 0 \tag{14c}$$

And in general for $r \geq 2$

$$\frac{\partial^2 u_{,r}}{\partial x^2} + \frac{1-\nu}{2}\frac{\partial^2 u_{,r}}{\partial y^2} + \frac{1+\nu}{2}\frac{\partial^2 v_{,r}}{\partial x\partial y}$$
$$= -\sum_{i=1}^{r-1} {}^rC_i\left[\frac{\partial w_{,r-i}}{\partial x}\frac{\partial^2 w_{,i}}{\partial x^2} + \frac{1-\nu}{2}\frac{\partial w_{,r-i}}{\partial x}\frac{\partial^2 w_{,i}}{\partial y^2} + \frac{1+\nu}{2}\frac{\partial w_{,r-i}}{\partial y}\frac{\partial^2 w_{,i}}{\partial x\partial y}\right] \tag{15a}$$

$$\frac{\partial^2 v_{,r}}{\partial y^2} + \frac{1-\nu}{2}\frac{\partial^2 v_{,r}}{\partial x^2} + \frac{1+\nu}{2}\frac{\partial^2 u_{,r}}{\partial x\partial y}$$
$$= -\sum_{i=1}^{r-1} {}^rC_i\left[\frac{\partial w_{,r-i}}{\partial y}\frac{\partial^2 w_{,i}}{\partial y^2} + \frac{1-\nu}{2}\frac{\partial w_{,r-i}}{\partial y}\frac{\partial^2 w_{,i}}{\partial x^2} + \frac{1+\nu}{2}\frac{\partial w_{,r-i}}{\partial x}\frac{\partial^2 w_{,i}}{\partial x\partial y}\right] \tag{15b}$$

$$D\nabla^4 w_{,r} - M_c\left[n^F_{xx,m}\frac{\partial^2 w_{,r}}{\partial x^2} + 2n^F_{xy,m}\frac{\partial^2 w_{,r}}{\partial x\partial y} + n^F_{yy,m}\frac{\partial^2 w_{,r}}{\partial y^2}\right]$$
$$= \sum_{i=1}^{r-1} {}^rC_i M_{,r-i}\left[n^F_{xx,m}\frac{\partial^2 w_{,i}}{\partial x^2} + 2n^F_{xy,m}\frac{\partial^2 w_{,i}}{\partial x\partial y} + n^F_{yy,m}\frac{\partial^2 w_{,i}}{\partial y^2}\right]$$
$$+\sum_{i=1}^{r-1} {}^rC_i\left\{k\left[\frac{\partial u_{,r-i}}{\partial x} + \nu\frac{\partial v_{,r-i}}{\partial y}\right]\frac{\partial^2 w_{,i}}{\partial x^2} + k\left[\frac{\partial v_{,r-i}}{\partial y} + \nu\frac{\partial u_{,r-i}}{\partial x}\right]\frac{\partial^2 w_{,i}}{\partial y^2}\right.$$
$$\left.+(1-\nu)k\left[\frac{\partial u_{,r-i}}{\partial y} + \frac{\partial v_{,r-i}}{\partial x}\right]\frac{\partial^2 w_{,i}}{\partial x\partial y}\right\}$$
$$+\sum_{i=1}^{r-1}\sum_{j=1}^{r-i-1} {}^rC_{ij}\left\{\frac{1}{2}k\left[\frac{\partial w_{,r-i-j}}{\partial x}\frac{\partial w_{,j}}{\partial x} + \nu\frac{\partial w_{,r-i-j}}{\partial y}\frac{\partial w_{,j}}{\partial y}\right]\frac{\partial^2 w_{,i}}{\partial x^2}\right.$$
$$+(1-\nu)k\frac{\partial w_{,r-i-j}}{\partial x}\frac{\partial w_{,j}}{\partial y}\frac{\partial^2 w_{,i}}{\partial x\partial y}$$
$$\left.+\frac{1}{2}k\left[\frac{\partial w_{,r-i-j}}{\partial y}\frac{\partial w_{,j}}{\partial y} + \nu\frac{\partial w_{,r-i-j}}{\partial x}\frac{\partial w_{,j}}{\partial x}\right]\frac{\partial^2 w_{,i}}{\partial y^2}\right\} \tag{15c}$$

where M_c is the critical moment,

$$u_{,r} = \frac{\mathrm{d}^r u}{\mathrm{d}\epsilon^r}\bigg|_{\epsilon=0}, \ldots\ldots$$

and

$${}^rC_i = \frac{r!}{(r-i)!i!}; \quad {}^rC_{ij} = \frac{r!}{(r-i-j)!j!i!}.$$

It has often been pointed out that there is some freedom in the choice of ϵ, but that no general rules can be devised to guide this. The choice in the present paper is

$$\epsilon = \bar{w} \tag{16a}$$

where $\bar{w}$ is the amplitude of the critical mode, so that

$$\bar{w}_{,1} = 1; \quad \bar{w}_{,2} = \bar{w}_{,3} = \cdots\cdots = \bar{w}_{,r} = \cdots = 0. \tag{16b}$$

It is apparent that eqns (14a) and (14b) are a set of homogeneous differential equations for which $(u_{,1}, v_{,1}) = (0,0)$. Solution of the eigenvalue eqn (14c) then yields the critical bending moment, M_c and the critical mode $w_{,1}$. In general the solution of the rth order perturbation eqns (15a) and (15b) is possible, after substitution of the known ith path derivatives, where $i = 1,2,\ldots,(r-1)$. However, the solution of eqn (15c) presents some problems because it requires the simultaneous determination of $M_{,r-1}$ and $w_{,r}$. A method of contraction has been proposed, both for discrete systems[11] and the present continuum system[10], that alleviates this problem. For the present problem this method reduces to the rth perturbation equation for $w_{,r}$ that is eqn (15c), being multiplied by $w_{,1}$; the product is then integrated over the domain of the structure and provided the equilibrium equations are derivable from a potential energy function (and in this case they are), the terms involving $w_{,r}$ drop out, leaving an explicit expression for $M_{,r-1}$ in terms of only known path derivatives[9]

$$M_{,r-1} = -\frac{I_2}{I_1} \tag{17}$$

where

$$I_1 = \int_{-L/2}^{+L/2}\int_0^d {}^rC_1\left[n^F_{xx,m}\frac{\partial^2 w_{,1}}{\partial x^2} + 2n^F_{xy,m}\frac{\partial^2 w_{,1}}{\partial x\partial y} + n^F_{yy,m}\frac{\partial^2 w_{,1}}{\partial y^2}\right] w_{,1}\,\mathrm{d}x\,\mathrm{d}y$$

$$-\int_{-L/2}^{+L/2} {}^rC_1\left[N^F_{x,m}\frac{\partial^2 w_{t,1}}{\partial x^2} - n^F_{yy,m}\frac{\partial w_{,1}}{\partial y}\right] w_{t,1}\bigg|_{y=d+{}^t t/2}\mathrm{d}x$$

$$-\frac{t_t}{2}\int_{-L/2}^{+L/2} {}^rC_1\left[n^F_{yy,m}\frac{\partial w_{,1}}{\partial y} + n^F_{xy,m}\frac{\partial w_{,1}}{\partial x}\right]\frac{\partial w_{t,1}}{\partial y}\bigg|_{y=d+{}^t t/2}\mathrm{d}x$$

$$-\frac{t_b}{2}\int_{-L/2}^{+L/2} {}^rC_1\left[n^F_{yy,m}\frac{\partial w_{,1}}{\partial y} + n^F_{xy,m}\frac{\partial w_{,1}}{\partial y}\right]\frac{\partial w_{b,1}}{\partial y}\bigg|_{y=-{}^t b/2}\mathrm{d}x$$

and

$$I_2 = \int_{-L/2}^{+L/2}\int_0^d \left\{\sum_{i=2}^{r-1} {}^rC_i M_{,r-i}\left[n^F_{xx,m}\frac{\partial^2 w_{,i}}{\partial x^2} + 2n^F_{xy,m}\frac{\partial^2 w_{,i}}{\partial x\partial y} + n^F_{yy,m}\frac{\partial^2 w_{,i}}{\partial y^2}\right]\right.$$

$$+\sum_{i=1}^{r-1} {}^rC_i\left\{k\left[\frac{\partial u_{,r-i}}{\partial x} + \nu\frac{\partial v_{,r-i}}{\partial y}\right]\frac{\partial^2 w_{,i}}{\partial x^2} + (1-\nu)k\left[\frac{\partial u_{,r-i}}{\partial y} - \frac{\partial v_{,r-i}}{\partial x}\right]\frac{\partial^2 w_{,i}}{\partial x\partial y}\right.$$

$$\left.\left. + k\left[\frac{\partial v_{,r-i}}{\partial y} + \nu\frac{\partial u_{,r-i}}{\partial x}\right]\frac{\partial^2 w_{,i}}{\partial y^2}\right\}\right.$$

$$+\sum_{i=1}^{r-1}\sum_{j=1}^{r-i-1} {}^{r}C_{ij}\left\{\frac{1}{2}k\left[\frac{\partial w_{,r-i-j}}{\partial x}\frac{\partial w_{,j}}{\partial x}+\nu\frac{\partial w_{,r-i-j}}{\partial y}\frac{\partial w_{,j}}{\partial y}\right]\frac{\partial^2 w_{,i}}{\partial x^2}\right.$$

$$+(1-\nu)k\frac{\partial w_{,r-i-j}}{\partial x}\frac{\partial w_{,j}}{\partial y}\frac{\partial^2 w_{,i}}{\partial x\partial y}$$

$$\left.+\frac{1}{2}k\left[\frac{\partial w_{,r-i-j}}{\partial y}\frac{\partial w_{,j}}{\partial y}+\nu\frac{\partial w_{,r-i-j}}{\partial x}\frac{\partial w_{,j}}{\partial x}\right]\frac{\partial^2 w_{,i}}{\partial y^2}\right\}\Bigg\} w_{,1}\,dx\,dy$$

$$-EA_t\int_{-L/2}^{+L/2}\left[\sum_{i=1}^{r-1}{}^{r}C_i\frac{\partial u_{t,r-i}}{\partial x}\frac{\partial^2 w_{t,i}}{\partial x^2}+\sum_{i=1}^{r-1}\sum_{j=1}^{r-i-1}{}^{r}C_{ij}\frac{1}{2}\frac{\partial w_{t,r-i-j}}{\partial x}\frac{\partial w_{t,j}}{\partial x}\frac{\partial^2 w_{t,i}}{\partial x^2}\right]w_{t,1}\Bigg|_{y=d+t_t/2}dx$$

$$+k\int_{-L/2}^{+L/2}\left\{\sum_{i=1}^{r-1}{}^{r}C_i\left[\frac{\partial v_{,r-i}}{\partial y}+\nu\frac{\partial u_{,r-i}}{\partial x}\right]\frac{\partial w_{,i}}{\partial y}\right.$$

$$\left.+\frac{1}{2}\sum_{i=1}^{r-1}\sum_{j=1}^{r-i-1}{}^{r}C_{ij}\left[\frac{\partial w_{,r-i-j}}{\partial y}\frac{\partial w_{,j}}{\partial y}+\nu\frac{\partial w_{,r-i-j}}{\partial x}\frac{\partial w_{,j}}{\partial x}\right]\frac{\partial w_{,i}}{\partial y}\right\}w_{t,1}\Bigg|_{y=d+t_t/2}dx$$

$$-\frac{t_t}{2}k\int_{-L/2}^{+L/2}\left\{\sum_{i=1}^{r-1}{}^{r}C_i\left\{\left[\frac{\partial v_{,r-i}}{\partial y}+\nu\frac{\partial u_{,r-i}}{\partial x}\right]\frac{\partial w_{,i}}{\partial y}+\frac{1}{2}(1-\nu)\left[\frac{\partial u_{,r-i}}{\partial y}+\frac{\partial v_{,r-i}}{\partial x}\right]\frac{\partial w_{,i}}{\partial x}\right\}\right.$$

$$+\sum_{i=1}^{r-1}\sum_{j=1}^{r-i-1}{}^{r}C_{ij}\left\{\frac{1}{2}\left[\frac{\partial w_{,r-i-j}}{\partial y}\frac{\partial w_{,j}}{\partial y}+\nu\frac{\partial w_{,r-i-j}}{\partial x}\frac{\partial w_{,j}}{\partial x}\right]\frac{\partial w_{,i}}{\partial y}\right.$$

$$\left.\left.+\frac{1}{2}(1-\nu)\frac{\partial w_{,r-i-j}}{\partial x}\frac{\partial w_{,j}}{\partial y}\frac{\partial w_{,i}}{\partial x}\right\}\right\}\frac{\partial w_{t,1}}{\partial y}\Bigg|_{y=d+t_t/2}dx$$

$$-\frac{t_b}{2}k\int_{-L/2}^{+L/2}\left\{\sum_{i=1}^{r-1}{}^{r}C_i\left\{\left[\frac{\partial v_{,r-i}}{\partial y}+\nu\frac{\partial u_{,r-i}}{\partial x}\right]\frac{\partial w_{,i}}{\partial y}+\frac{1}{2}(1-\nu)\left[\frac{\partial u_{,r-i}}{\partial y}+\frac{\partial v_{,r-i}}{\partial x}\right]\frac{\partial w_{,i}}{\partial x}\right\}\right.$$

$$+\sum_{i=1}^{r-1}\sum_{j=1}^{r-i-1}{}^{r}C_{ij}\left\{\frac{1}{2}\left[\frac{\partial w_{,r-i-j}}{\partial y}\frac{\partial w_{,j}}{\partial y}+\nu\frac{\partial w_{,r-i-j}}{\partial x}\frac{\partial w_{,j}}{\partial x}\right]\frac{\partial w_{,i}}{\partial y}\right.$$

$$\left.\left.+\frac{1}{2}(1-\nu)\frac{\partial w_{,r-i-j}}{\partial x}\frac{\partial w_{,j}}{\partial y}\frac{\partial w_{,i}}{\partial x}\right\}\right\}\frac{\partial w_{b,1}}{\partial y}\Bigg|_{y=-t_b/2}dx$$

$$-\int_{-L/2}^{+L/2}\sum_{i=2}^{r-1}{}^{r}C_iM_{,r-i}\left\{\left[N^F_{x,m}\frac{\partial^2 w_{t,i}}{\partial x^2}-n^F_{yy,m}\frac{\partial w_{,i}}{\partial y}\right]w_{t,1}\right.$$

$$\left.+\frac{t_t}{2}\left[n^F_{yy,m}\frac{\partial w_{,i}}{\partial y}+n^F_{xy,m}\frac{\partial w_{,i}}{\partial x}\right]\frac{\partial w_{t,1}}{\partial y}\right\}\Bigg|_{y=d+t_t/2}dx$$

$$-\frac{t_b}{2}\int_{-L/2}^{+L/2}\sum_{i=2}^{r-1}{}^{r}C_iM_{,r-i}\left[n^F_{yy,m}\frac{\partial w_{,i}}{\partial y}+n^F_{xy,m}\frac{\partial w_{,i}}{\partial x}\right]\frac{\partial w_{b,1}}{\partial y}\Bigg|_{y=-t_b/2}dx.$$

Once $M_{,r-1}$ is determined it is possible to solve the full eqn (15c) to obtain path derivative $w_{,r}$. This perturbation sequence, depicted in Fig. 6, can then continue on a similar pattern until the number of load and displacement path derivatives necessary for acceptable convergence has been reached.

It can be shown from the preceeding analysis that odd path derivatives of M, u and v and even path derivatives of w vanish. This can be explained physically by the nature of the problem, in that the behaviour of the model is independent of the sign of $\epsilon \equiv \bar{w}$. This implies expansions of the form

$$M = M_c + \frac{1}{2}M_{,2}\epsilon^2 + \frac{1}{24}M_{,4}\epsilon^4 + \frac{1}{720}M_{,6}\epsilon^6 + \cdots \tag{18a}$$

$$U = U^F + \frac{1}{2}u_{,2}\epsilon^2 + \frac{1}{24}u_{,4}\epsilon^4 + \frac{1}{720}u_{,6}\epsilon^6 + \cdots \tag{18b}$$

$$V = V^F + \frac{1}{2}v_{,2}\epsilon^2 + \frac{1}{24}v_{,4}\epsilon^4 + \frac{1}{720}v_{,6}\epsilon^6 + \cdots \tag{18c}$$

$$W = w_{,1}\epsilon + \frac{1}{6}w_{,3}\epsilon^3 + \frac{1}{120}w_{,5}\epsilon^5 + \cdots \tag{18d}$$

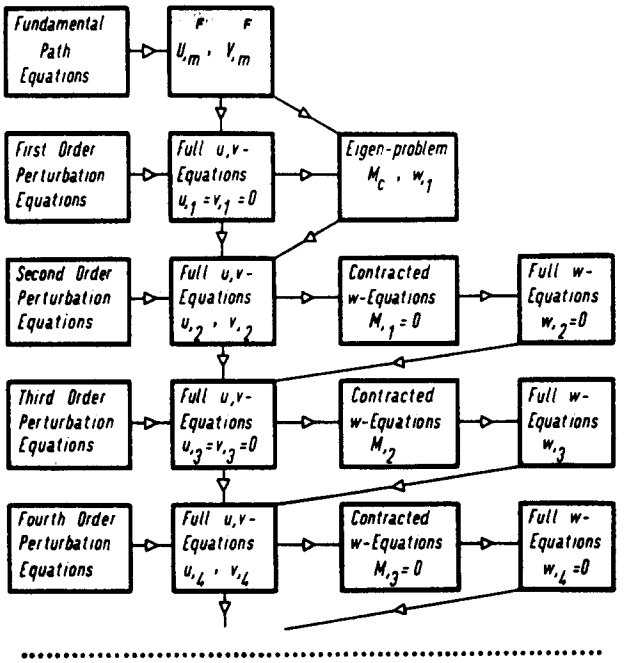

Fig. 6. Sequence of operations in perturbation analysis.

The boundary conditions are treated in a similar way, so that when solved together with the corresponding perturbed equilibrium equations they yield the required solution to the problem.

5. NUMERICAL ANALYSIS

Finite differences model

To facilitate solution the linearised perturbation equations are discretized by replacing the partial derivatives by pertinent difference expressions.

A rectangular grid is superimposed on the plate with grid spacings given by $h_x = L/m$ and $h_y = d/n$, where m and n are respectively the number of spacings in the x and y coordinate directions.

The fundamental path displacement components (U^F, V^F) are defined inside the domain of differential dependance by the application of finite differences approximations, involving error terms of order (h^2), of the equilibrium eqns (11). It is found that the application of these equations requires the definition of displacement components at nodal points outside the physical domain of the problem. These so called ficticious generalised coordinates are defined by the application of higher order finite difference approximations, with truncation errors of order (h^4), of the perturbed form of boundary conditions (8)–(10) at the nodal points on the boundaries [9].

Solution of the fundamental path difference equations

Application of the fundamental path difference expressions in the manner described above results in a set of linear algebraic simultaneous equations of the form

$$[A_u]\{U^F\} = \{q_u{}^F\} \tag{19}$$

where $[A_u]$ is the matrix of coefficients and $\{U^F\}$ and $\{q_u{}^F\}$ are vectors containing displacement

solution of the postcritical path equations. It is therefore felt that the method employed for the solution of eqn (19) should take advantage of this property of $[A_u]$ for computational efficiency. Iterative methods of solution had to be excluded, since for each new r.h.s. vector the iterative process has to be started from the beginning, thus requiring large amounts of computing time. A direct method is therefore chosen for the solution of the present problem [12], in which the

sparseness of $[A_w]$ is utilised by using an efficient indexing format, so that only non-zero matrix elements need to be in store before and after decomposition.

Solution of the eigen-problem

The finite difference model required for the solution of the eigen-problem can be constructed in the manner described earlier, by the application of the finite difference approximation of the first order perturbation eqn (14c) inside the physical domain of the problem, and of the perturbed form boundary conditions (8b), (8c), (9b), (9c), (10c) and (10d) on the corresponding boundaries. The resulting system of linear algebraic simultaneous equations can then be written in the form

$$[A_L]\{w_{,1}\} = M_c[A_R]\{w_{,1}\} \tag{20}$$

$[A_L]$ and $[A_R]$ are matrices of coefficients of the system of equations; $\{w_{,1}\}$ is a vector of discretized displacement components $w_{,1}$.

An inverse iteration method [9, 13] has been used for the solution of eigen-equation (20).

Solution of the postcritical path equations

The solution of the postcritical problem consists of three distinct parts in a natural sequence, depicted in Fig. 6. In the first, the general u and v-perturbation eqns (15a) and (15b) are solved for $r = 2, 4, \ldots$ In the second, the contracted eqn (17) is used to obtain the load path derivatives $M_{,r-1}$ with $r = 3, 5, \ldots$ And finally in the third part the general w-perturbation eqn (15c) is solved with $r = 3, 5, \ldots$

Discretization of the rth order u and v-perturbation equations and the appropriate boundary conditions, results in a system of linear simultaneous algebraic equations of the same form as eqn (19). The r.h.s. vector is now a function of known path derivatives of $w_{,k}$; $k = 1, 3 \ldots, r-1$, that have been found from the solution of the previous kth order perturbation equations.

However, the solution of the contracted eqn (17) requires the evaluation of surface integrals inside the physical domain of the problem and line integrals on the boundaries. This has been achieved by the use of a two-dimensional form of Simpson's integration rule, in which the functionals inside the surface integrals are computed numerically at each of the nodal points, while the functionals inside the line integrals are computed at the nodal points on the boundaries. The partial differentials are discretized using difference expressions of order (h^4).

With $M_{,r-1}$ known, discretization of the rth order w-perturbation equation and the corresponding boundary conditions results in a system of linear simultaneous algebraic equations of the form

$$[A_w]\{w_{,r}\} = \{q_w{}^r\} \tag{21}$$

where $[A_w]$ is the matrix of coefficients of the system of equations, $\{w_{,r}\}$ is a vector of the discretized displacement path derivatives $w_{,r}$, and $\{q_w{}^r\}$ is a vector of equivalent loading components, represented by the discretized r.h.s. of the rth order w-perturbation eqn (15c).

It is evident by inspection of eqns (14c) and (15c) that

$$[A_w] = [A_L] - M_c[A_R] \tag{22}$$

so that $[A_w]$ can be conveniently obtained using eqn (22) immediately after the solution of the eigen-problem, without having to re-compute the coefficients of the discretized system of the rth order perturbation equations. Matrix $[A_w]$ in the form given by eqn (22) is singular. It is transformed into a non-singular form with the convenient choice of perturbation parameter $\epsilon \equiv \bar{w}$, as described earlier. Solution of eqn (21) is then achieved using the same direct matrix solution method [12] that was used for the fundamental path.

6. ACCURACY OF DIFFERENCE SOLUTIONS

Assuming that the behaviour of the structural system under investigation is represented sufficiently accurately by the equilibrium equations and boundary conditions developed in Section 4, the main sources of error that could affect the accuracy of the numerical solutions are truncation errors due to the discretization of the equilibrium equations and the boundary conditions. A number of researchers that have worked with finite differences approximations [14, 15], examined the effects of these errors in assessing the numerical accuracy of their solutions. In general, it has been found[9] that employing higher order boundary analogues results in superior convergence rates, in comparison with ordinary finite differences approximations on the boundaries.

To demonstrate the importance of truncation errors arising from the finite difference discretization of the differential equations, convergence studies were carried out on several models with varying geometries, yielding much the same results. The following typical results relate to a model with lateral stiffener spacing $L = 120.0$ mm, stiffener depth $d = 60.0$ mm and stiffener thickness $t = 1.50$ mm. The flange plate dimensions are $b_b = 90.0$ mm and $t_b = 1.50$ mm. In the case of a top beam $b_t = 5.0$ mm and $t_t = 7.5$ mm. The material properties are $E = 3100\ \text{N/mm}^2$ and $\nu = 0.40$. Solutions were obtained on grids chosen with $n = 4, 6, 8, 10, 12$ and for all cases $m = 2n$.

Torsional stiffnesses of the bottom flange plate and the top beam, appearing in eqns (9b) and (8b), are given by

$$GJ_b = \frac{E}{2(1+\nu)}\frac{1}{3}C_b \min(b_b t_b^3, t_b b_b^3) \tag{23}$$

$$GJ_t = \frac{E}{2(1+\nu)}\frac{1}{3}C_t \min(b_t t_t^3, t_t b_t^3) \tag{24}$$

where[16]

$$C_b = 1 - \frac{192}{\pi^5}\frac{1}{s_b}\sum_{n=1,3,\ldots}^{\infty}\frac{1}{n^3}\tanh\left(\frac{n\pi}{2}s_b\right); \quad s_b = \max\left(\frac{b_b}{t_b}, \frac{t_b}{b_b}\right)$$

and

$$C_t = 1 - \frac{192}{\pi^5}\frac{1}{s_t}\sum_{n=1,3,\ldots}^{\infty}\frac{1}{n^3}\tanh\left(\frac{n\pi}{2}s_t\right); \quad s_t = \max\left(\frac{b_t}{t_t}, \frac{t_t}{b_t}\right).$$

These particular dimensions and material properties have been chosen so as to correspond with the experimental model results referred to in the following section.

The converegence rate is examined by investigating the out-of-plane displacement amplitude, $\bar{w}$, and the overall curvature, κ, at $x = 0$ (see Fig. 2), when plotted against the externally applied bending moment, M, shown in Figs. 7 and 8.

The curvature, κ, of the theoretical and experimental model is defined as the slope of the axial strain distribution, over a section in the longitudinal stiffener, evaluated at $(x, y) = (0, 0)$. The reason for choosing this position is to ensure that the strains are in the tension field where the strain distribution remains effectively linear after local torsional buckling occurs[9]. Therefore

$$\kappa = \left.\frac{\partial e_{xx}}{\partial y}\right|_{x=y=0} \tag{25}$$

where

$$e_{xx} = \frac{\partial U}{\partial x} + \frac{1}{2}\left(\frac{\partial W}{\partial x}\right)^2.$$

It has been demonstrated[9] that this experimentally convenient measure of local curvature is within 4% of the overall curvature measured by the relative rotations of the end boundaries at $x = \pm L/2$.

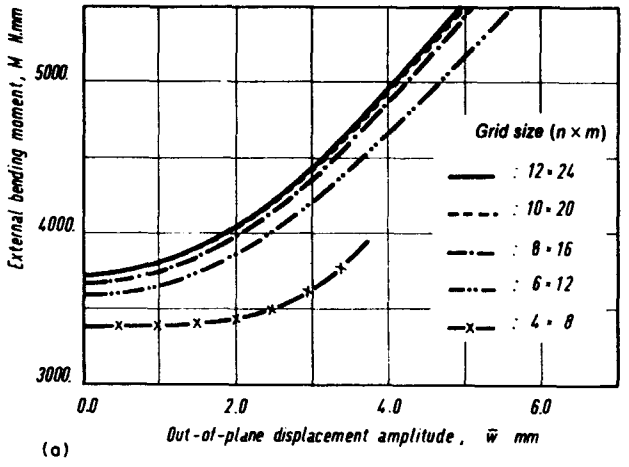

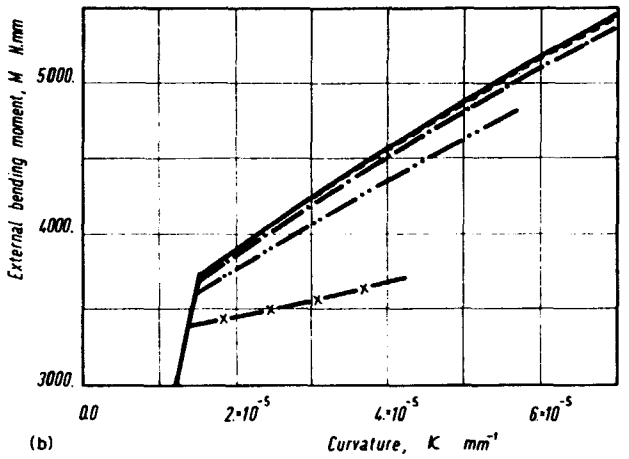

Fig. 7. Convergence studies for a model with a free top longitudinal boundary.

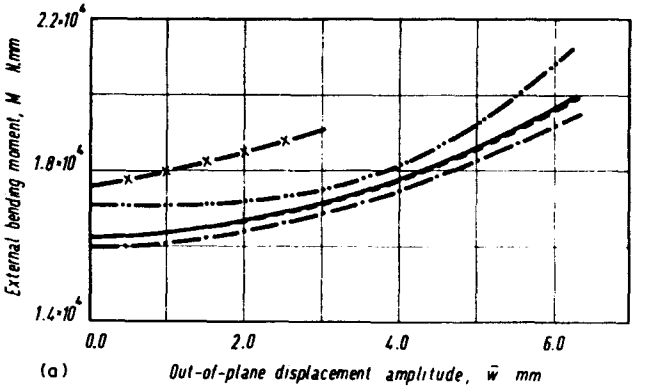

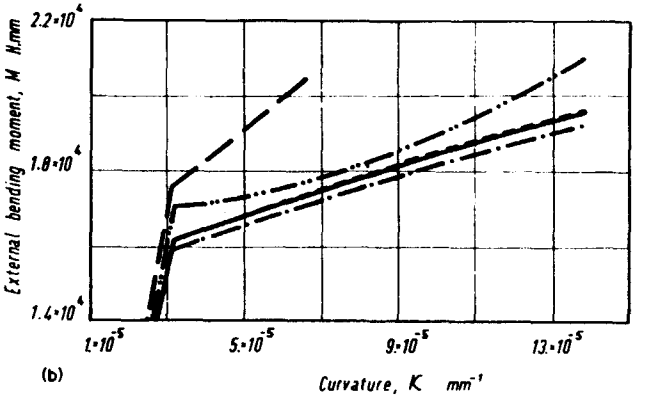

Fig. 8. Convergence studies for model with a beam supported top longitudinal boundary. Key as for Fig. 7.

It can be seen that for all cases the curves corresponding with $n = 10$ and $n = 12$ almost exactly coincide, and therefore a grid with $n = 12$ can be considered to yield effectively converged results.

Truncation of the perturbation series expansions (18) up to and including the sixth order term, has been found to be sufficient in providing converged results.

7. TYPICAL THEORETICAL RESULTS AND COMPARISON WITH EXPERIMENTS

Simple small scale Araldite models, similar in shape to the model described in Fig. 2, were tested to verify experimentally the validity of the theoretical results. Detailed description of the experimental set-up, procedures and results is given in Ref. [9]. In the theoretical analysis the torsional stiffness of the bottom beam was chosen as described by eqn (23) to correspond to the experimental model conditions. The models were tested under pure bending moments.

A comparison between the present theoretical solutions and experimental results is presented in Figs. 9 and 10 for models with free and beam supported top longitudinal boundaries respectively. The parameters plotted against the externally applied bending moment, M, are the out-of-plane displacement amplitude, $\bar{w}$ and the curvature, κ, at $(x, y) = (0, 0)$. The close agreement between theory and experiments indicates that the assumptions made in the analysis are justified. In particular, the assumptions made concerning the beam-plate interactions and compatibility of displacements produce results that compare well with experimental conditions.

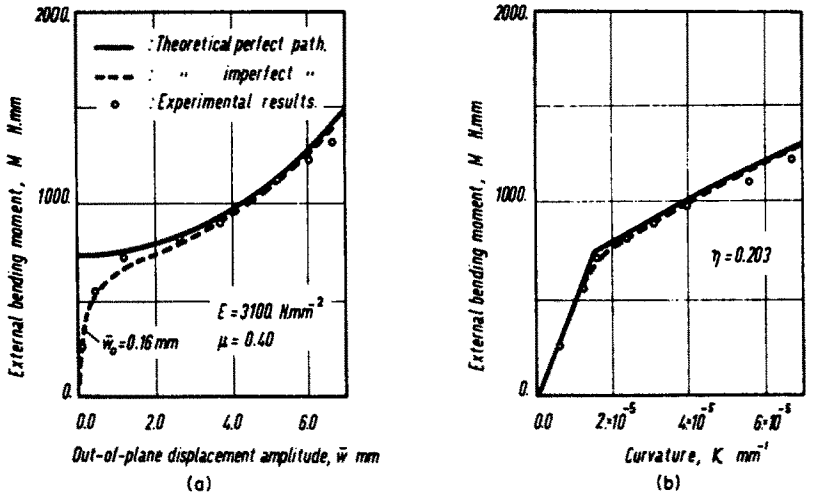

Fig. 9. Comparison of theoretical and experimental results for a model with $L = 125.0$ mm, $d = 74.0$ mm, $t = 1.80$ mm, $b_b = 100.0$ mm and $t_b = 1.73$ mm.

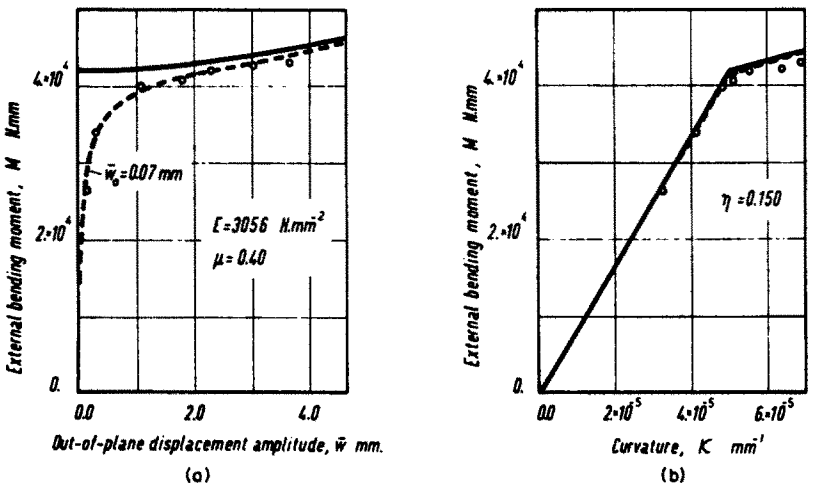

Fig. 10. Comparison of theoretical and experimental results for a model with $L = 125.0$ mm, $d = 59.0$ mm, $t = 1.80$ mm, $b_b = 100.0$ mm, $t_b = 1.73$ mm, $b_t = 5.15$ mm and $t_t = 15.10$ mm. Key as for Fig. 9.

It should also be noted here that although the torsional stiffness of the bottom beam, as given by eqn (23), has been chosen to model the action of the experimental model, a simple modification can allow it to also model the case of continuity shown in Fig. 1(c).

An additional important result that emerged from a study in which the externally applied axial load, P, was varied systematically over a wide range for a series of models, was that it produced no significant changes in the pre- and postcritical moment-curvature relationship, apart from affecting the level of the critical bending moment, M_c. The results of this study are summarised in Fig. 11 for the model described in the previous section. It would appear that the reduced modulus factor, η, which is defined as the ratio of the post-to the precritical slopes of the moment-curvature graph, is independent of the location of the system within the axial load-deformation space. Also shown in Fig. 11 is the relative insensitivity of η to large deformations.

An extensive parametric study[9] showed that the reduced modulus factor for stiffened plates is very low, being in general under 0.25. This severity in the reduction of η is due to the fact that the bending stiffness of such structures is mainly controlled by the contribution to the overall second moment of area of the section from the stiffener outstands. So, when the stiffeners buckle torsionally and their effective contribution decreases considerably, it causes dramatic reductions in the overall bending stiffness and therefore the reduced modulus factor. This reduction becomes even more severe in the presence of a top longitudinal beam; the reason being that the considerable contribution of the top beam to the second moment of area of the section is almost completely lost after buckling. This is highlighted by comparing Figs. 9 and 10; it is shown that the addition of a top longitudinal beam to the experimental model resulted in an even further reduction in η, from 0.203 to 0.150. These reductions in the reduced modulus factors of such structures are indicative of the potentially severe imperfection sensitivity that may arise when axially loaded stiffened plate buckling involves an unstable coupling between the overall plate mode and a local torsional stiffener mode.

8. CONCLUSIONS

The theoretical non-linear large deflection equations governing the elastic behaviour of the analytical models and special equilibrium and compatibility equations developed to formulate theoretically the plate-beam boundary conditions, have been presented.

A linear sequence of perturbation equations has been derived to replace the non-linear differential equations, using a continuum perturbation approach. They were subsequently discretized by the introduction of pertinent difference expressions. Following the example of other researchers, higher order differences have been used to discretize the boundary conditions. It was found that in general this resulted in improved convergence to the exact solutions as difference grids were refined, with insignificantly increases in computational effort.

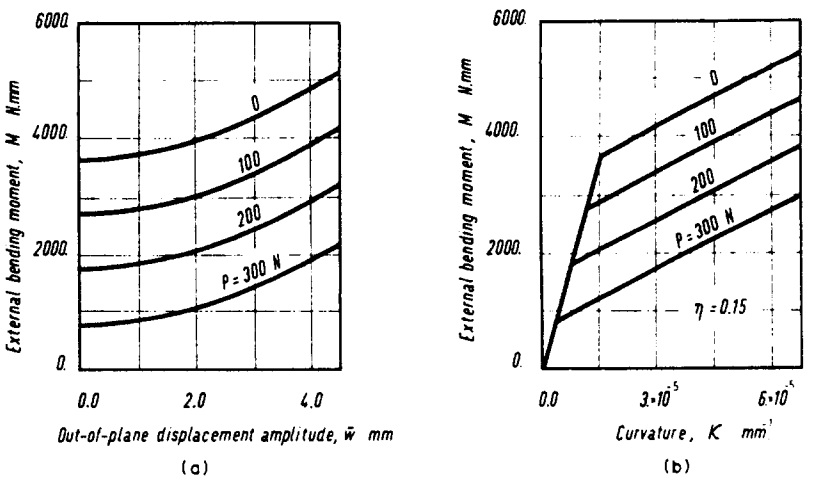

Fig. 11. Influence of externally applied axial compressive force, P, on the critical moment and postcritical behaviour.

Comparison with experimental results shows good agreement, even in the advanced post-critical range, indicating that the theoretical analysis developed in this paper predicts accurately the behaviour of the physical models.

However, the importance of the present results is that the accurate prediction of the moment-curvature relationship enables the calculation of the reduced modulus factor for these models. Its significance is very evident in the analysis of systems that undergo interactive buckling. Particularly, in the case of stiffened plates buckling away from slender longitudinal stiffener outstands, the present results can be usefully employed as the basis in deriving simple engineering approaches, that may avert the necessity of performing highly nonlinear interactive buckling analyses.

REFERENCES

1. A. Van der Neut, The interaction of local buckling and column failure of thin-walled compression members *Proc. of 12th Intern. Congress Appl. Mech.* pp. 389–399 Springer Berlin (1969).
2. V. Tvergaard, Imperfection sensitivity of a wide integrally stiffened panel under compression. *Int. J. Solids Structures* 9, 177–192 (1973).
3. W. T. Koiter and M. Pignataro, A general theory for the interaction between local and overall buckling of stiffened plates. *Final Rep.* 556. *Lab. of Eng. Mech.* Mekelweg 2, Delft, Holland, (1976).
4. C. P. Ellinas, P. Kaoulla, S. Kattura and J. G. A. Croll, Tests on interactive buckling of stiffened plates. *Exp. Mech.* 17, 455–462 (1977).
5. G. H. Little, Stiffened compression panels–theoretical analysis *The Struct. Engng* 54, 489–500 (1976).
6. J. M. T. Thompson, J. D. Tulk and A. C. Walker, An experimental study of imperfection sensitivity in the interactive buckling of stiffened plates. *Proc. of I.U.T.A.M., Symp. of the Buckling of Structures.* Springer–Verlag Harvard, (1976).
7. J. G. A. Croll, Model of interactive buckling of stiffened plates. *Proc. of A.S.C.E., Eng. Mech. Div.* EM5, 101, 575–591 (1975).
8. S. E. Svenson and J. G. A. Croll, Interaction between local and overall buckling. *Int. J. Mech. Sci.* 17, 307–321 (1975).
9. C. P. Ellinas, Moment-curvature characteristics of locally buckled stiffened plates Ph.D. Thesis. University College, London (1978).
10. J. G. A. Croll, Continuum perturbation method in the branching analysis of conservative systems. *Int. J. Mech. Sci.* 13, 605–613 (1971).
11. J. M. T. Thompson, An introduction to elastic stability. *Structural Instability* (Edited by W. J. Supple). IPC Science and Technology Press (1973).
12. A. R. Curtis and J. K. Reid, Fortran subroutines for the solution of sparse sets of linear equations *Rep. R6844, A.E.R.E.* Harwell, England (1971).
13. J. H. Wilkinson, *The Algebraic Eigenvalue Problem.* University Press, Oxford (1968).
14. M. Abramowitz and W. F. Cahill, On the vibration of a square clamped plate. *J. Assoc. Computer Machinery* 2, 162–168 (1955).
15. A. K. Noor, Mixed finite difference scheme for analysis of simply supported thick plate. *Comput. Struct.* 3, 967–982 (1973).
16. S. Timoshenko and J. N. Goodier, *Theory of Plates and Shells.* McGraw-Hill, New York (1959).